ACS SENSORS

pubs.acs.org/acssensors
Article

CRISPR-Based Assay for Point-of-Care Pharmacogenetic CYP2C19 Genotyping

Published as part of ACS Sensors special issue "CRISPR in Sensing".

Alexander J. Schubert,[†] Qiyao Meng,[†] Joshua Hoffmann, Josefine Rau, Fabian Abele, Robert Greensmith, Carlos Cordero, Antonia Ibel, Julia M. Mandler, Kai-Uwe Eckardt, Jan Halbritter, Anand S. Dighe, Xiao Tan, Daw-Yang Hwang, Tobias Petzold, Philipp Enghard, and Michael M. Kaminski*

Cite This: https://doi.org/10.1021/acssensors.6c00841

Read Online

ACCESS | Metrics & More | Article Recommendations | Supporting Information

ABSTRACT: Pharmacogenetic testing enables personalized drug dosing by accounting for genetic variation in drug metabolism. Although there is increasing evidence that genetically guided dosing improves therapeutic efficacy and reduces adverse effects, clinical implementation remains limited as genotyping methods suffer from slow turnaround times and are not optimized for point-of-care use. Here, we present a rapid, multiplexed CRISPR-based assay for genotyping the key CYP2C19 polymorphisms *2, *3, and *17. These variants can alter enzyme activity, impacting the metabolism of drugs such as clopidogrel and mavacamten. Our assay combines isothermal amplification with a dual guide RNA detection strategy, where LwaCas13a selectively detects mutant alleles and LbaCas12a identifies wild-type alleles. In a validation study of 110 participants, the assay showed high concordance with Sanger sequencing, the current gold standard, with variant-specific accuracies of 97.3% (*2), 100% (*3), and 99.1% (*17), demonstrating robust performance across a diverse clinical cohort. The workflow supports both column-based DNA extraction and a simplified, crude extraction protocol. Genotyping results are obtained through either fluorescence detection or multi-analyte lateral-flow readouts, allowing visual interpretation of genotypes with minimal equipment. In conclusion, our findings show that CRISPR-based genotyping can deliver accurate CYP2C19 pharmacogenetic testing, facilitating broader adoption of genotype-guided drug dosing. Furthermore, the programmability of CRISPR-Cas systems enables adaptation to other pharmacogenetic targets relevant to drug metabolism.

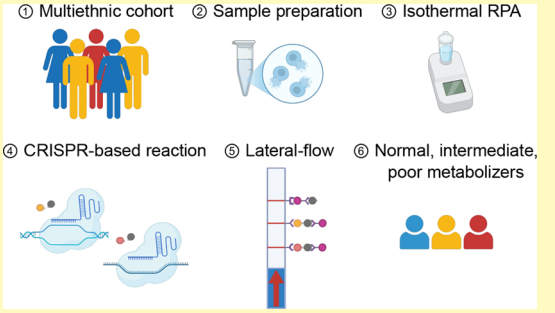

KEYWORDS: *CRISPR-based diagnostics, LwaCas13a, LbaCas12a, CYP2C19 genotyping, isothermal amplification, multi-analyte lateral-flow readout, clopidogrel, mavacamten*

Pharmacogenetics aims to personalize drug therapy by investigating the influence of genetic variation on drug metabolism, efficacy, and safety. Although polymorphisms have been reported in dozens of enzymes, only a subset, including CYP2C19, CYP2D6, CYP2C9, and DPYD, are currently considered clinically actionable.[1] Among these, CYP2C19 stands out as a key example where genotyping directly informs dosing decisions.[2] Common CYP2C19 single nucleotide polymorphisms (SNPs) include the loss-of-function alleles CYP2C19*2 (rs4244285) and CYP2C19*3 (rs4986893) and the gain-of-function allele CYP2C19*17 (rs12248560), with global average allele frequencies of 15.2, 0.3, and 20.4%, respectively; these frequencies vary considerably across populations.[2,3] CYP2C19 alone contributes to the metabolism of around ten percent of commonly prescribed drugs,[4] and more than half of individuals carry at least one gain-of-function or loss-of-function CYP2C19 allele,[3] underscoring the need for rapid genotyping in routine care. Individuals with two loss-of-function alleles (e.g., *2/*3) are classified as poor metabolizers (PMs), while those with one such allele are classified as intermediate metabolizers (IMs) (Figure 1a).[2] Heterozygous (HET) patients (e.g., *1/*17) of the CYP2C19*17 gain-of-function allele are classified as rapid metabolizers (RMs), whereas homozygous mutant (MUT) carriers (*17/*17) are classified as ultrarapid metabolizers (UMs).[2] In contrast, wild-type (WT) patients (*1/*1) for the CYP2C19 gene are classified as normal metabolizers (NMs).[2]

CYP2C19 genotyping has been extensively studied to guide oral P2Y12 inhibitor therapy in cardiovascular disease, particularly clopidogrel, whose metabolic bioactivation is

Received: February 25, 2026
Revised: May 22, 2026
Accepted: May 29, 2026

https://doi.org/10.1021/acssensors.6c00841
ACS Sens. XXXX, XXX, XXX−XXX

a

Phenotype	Genotype	Therapeutic recommendation	
Ultrarapid	*17/*17	If considering clopidogrel, use at standard dose.	If considering mavacamten, use at standard dose.
Rapid	*1/*17		
Normal	*1/*1		
Intermediate	*1/*2, *1/*3, *2/*17, *3/*17	Avoid clopidogrel if possible. Use prasugrel or ticagrelor at standard dose if possible.	
Poor	*2/*2, *2/*3, *3/*3		If considering mavacamten, use at reduced dose.

b

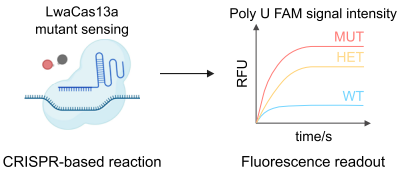

c

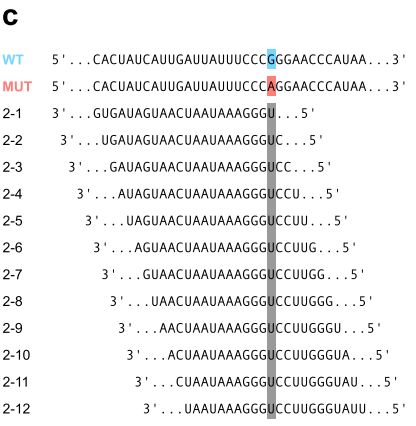

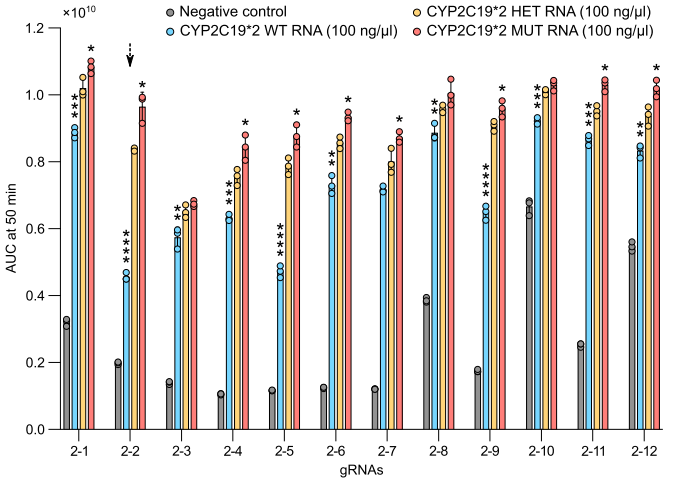

d

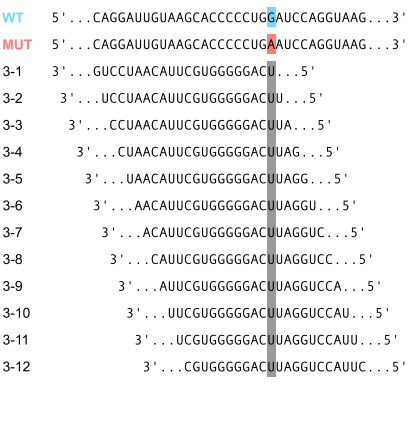

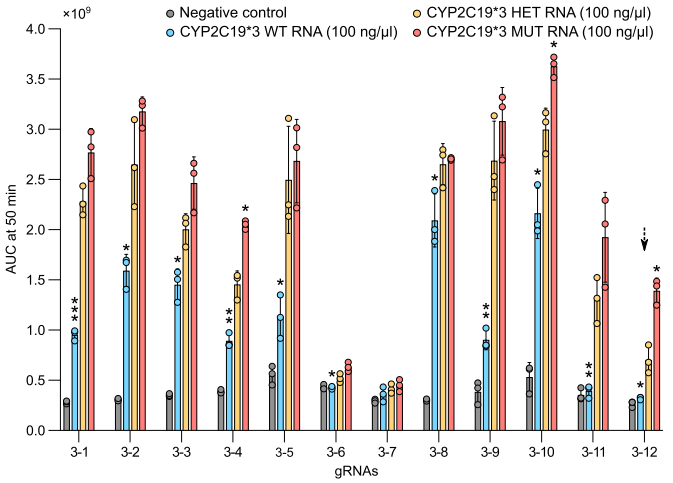

e

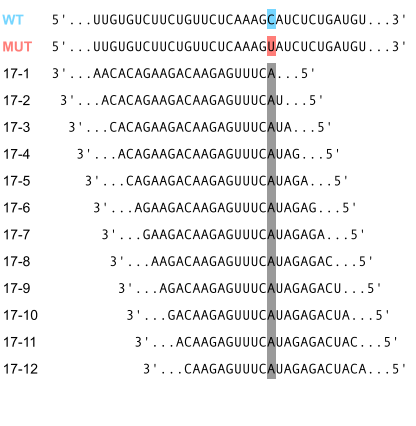

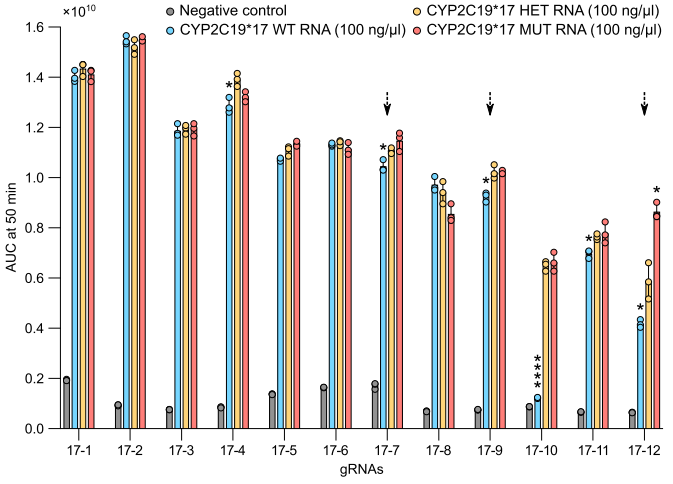

Figure 1. Systematic gRNA screen for rapid CYP2C19 genotyping on synthetic RNA targets. (a) Overview of CYP2C19 phenotypes, genotypes, and therapeutic recommendations for clopidogrel and mavacamten use.[2,12] (b) Illustration of the systematic gRNA screen. Synthetic RNA

https://doi.org/10.1021/acssensors.6c00841
ACS Sens. XXXX, XXX, XXX−XXX

Figure 1. continued

targets undergo CRISPR-based detection with LwaCas13a and a MUT-sensing gRNA. Fluorescence is measured using a poly U FAM reporter oligonucleotide. (c–e) Left: Alignment of target sequences and design of 12 different LwaCas13a MUT-sensing gRNAs for CYP2C19*2 (c), *3 (d), and *17 (e). The WT sequence is highlighted in blue, the MUT sequence in red, and the position of the SNP in dark gray. Right: Bar graphs showing the fluorescence signal of the tested gRNAs for CYP2C19*2 (c), *3 (d), and *17 (e). $n = 3$ technical replicates. Synthetic RNA targets at 100 ng/μL. Bar graphs indicate mean ± SD. $P < 0.05$ (*), $P < 0.01$ (**), $P < 0.001$ (***), and $P < 0.0001$ (****). Selected gRNAs for further optimization are marked by dashed arrows.

CYP2C19-dependent.[5] Genotype-guided antiplatelet selection helps balance ischemic and bleeding risk.[2] Notably, clopidogrel-treated IMs or PMs have about a 50 percent higher risk of cardiovascular events and a roughly threefold higher risk of stent thrombosis after percutaneous coronary intervention (PCI) compared with non-carriers.[6−9] Accordingly, the POPular Genetics and TAILOR-PCI trials support using prasugrel or ticagrelor in patients with reduced CYP2C19 activity.[10,11] Moreover, CYP2C19 genotyping is also recommended prior to initiating mavacamten for the treatment of hypertrophic obstructive cardiomyopathy (HOCM), as PMs exhibit higher drug exposure and an increased risk of systolic dysfunction.[12−14] To mitigate these adverse effects, the current European product information recommends CYP2C19 genotyping before initiating mavacamten.[12,15]

Despite encouraging clinical evidence and guidelines, CYP2C19 genotyping implementation in clinical routine remains limited.[2,16] Conventional techniques like Sanger sequencing are costly, time-consuming, and infrastructure reliant, restricting decentralized use.[17] CRISPR-based diagnostics offer a promising alternative for SNP detection due to their speed, accuracy, and simplicity.[18,19] While point-of-care CRISPR diagnostics are emerging,[20−22] many current assays lack true sample-to-answer workflow and still require multistep extraction or specialized equipment, limiting point-of-care use.[17,23,24] CRISPR-based CYP2C19 genotyping assays often rely on PCR preamplification, column-based sample preparation, or complex readouts, hindering widespread use.[25−30] Furthermore, validation in large and geographically diverse clinical cohorts is an important next step.[17]

To address these limitations, we developed a rapid isothermal CRISPR-based CYP2C19 genotyping assay optimized for high-throughput compatible fluorescence readouts, and extended the assay to support simplified crude extraction and portable immunochromatographic strips for decentralized testing. We systematically evaluated guide RNA (gRNA) designs and assay configurations to reliably distinguish WT, HET, and MUT genotypes across all common CYP2C19 variants. The method was validated in a geographically diverse multicenter clinical cohort that included individuals with rare alleles and demonstrated strong diagnostic performance for pharmacogenetic testing.

■ MATERIALS AND METHODOLOGY

Primer Design

CYP2C19 genetic variants were selected according to the CYP2C19 CPIC guideline.[2] The positions of the selected variants (CYP2C19*2, *3, and *17) inside the CYP2C19 gene were identified using the *National Center for Biotechnology Information* database. The design of the forward primer (FP) and reverse primer (RP) for recombinase polymerase amplification (RPA) was carried out using the PRIMER-BLAST application with the parameters specified in the SHERLOCK protocol.[31−33] A T7 promoter (T7P) sequence was appended to the 5' end of the RPA FP to allow T7 transcription, unless specified otherwise.[31−33]

gRNA Design and Production

gRNAs for LwaCas13a and LbaCas12a were designed based on the SHERLOCK protocol, to contain spacers of 28 and 20 nucleotides, respectively, each complementary to the target sequence.[31−33] DNA oligos (Eurofins) containing a T7P sequence were used as templates for in vitro transcription of gRNAs with the HiScribe T7 Quick High Yield RNA Synthesis Kit (NEB) and subsequently purified using the RNA Clean & Concentrator 25 kit (Zymo Research) according to the manufacturer's instructions. The direct repeat was positioned at the 5′ end of the spacer.[31−33]

Reporter Molecules

For fluorescence-based detection, reporter oligonucleotides were designed to include sequences recognized and cleaved by each Cas enzyme: AU or UUUUU for LwaCas13a and TTATT for LbaCas12a.[31−33] Reporters were labeled with a fluorophore and quencher pair (Texas Red, hexachlorofluorescein [HEX], or FAM) and synthesized as RNA or ssDNA (IDT).[31−33] For lateral-flow readout, reporters were dual-labeled with FAM and biotin (for LwaCas13a) or FAM and digoxigenin (for LbaCas12a).[31−33]

LwaCas13a, LbaCas12a, and Target RNA Production

The expression vector pC013-Twinstrep-SUMO-huLwaCas13a (Addgene plasmid #90097, RRID: Addgene_90097) was a gift from Feng Zhang.[31−33] LbaCas12a was produced by New England Biolabs (NEB, M0653T), while LwaCas13a was produced and purified as described previously.[22] DNA gBlocks gene fragments (IDT) containing a T7P sequence were used as templates for in vitro transcription of synthetic RNA targets using the HiScribe T7 Quick High Yield RNA Synthesis Kit (NEB) and purified using the RNA Clean & Concentrator 25 kit (Zymo Research) according to the manufacturer's instructions.

RPA Reaction

RPA reactions were conducted for 1 h at 39 °C in a total volume of 20 μL, using either the TwistAmp Basic kit (TwistDx) or the multienzyme isothermal rapid amplification kit (MIRA, AmpFuture Biotech), with 2 μL of DNA serving as the sample input. For TwistDx, each reaction contained 0.267× pellet, 480 nM FPs and RPs, 11.8 μL of rehydration buffer, and 8 mM magnesium acetate. For MIRA, each reaction contained 0.4× pellet, 400 nM FPs and RPs, 11.8 μL of Buffer A, and 1 μL of Buffer B.

CRISPR-Cas-Based Reaction

RNA and DNA detections were performed using a modified SHERLOCK protocol.[31−33] For LwaCas13a RNA detection, reactions (20 μL) contained 3 μL of synthetic RNA targets, murine RNase inhibitor (1 U/μL), NEBuffer 2.1 (1×), LwaCas13a (45 nM), background total human RNA purified from human embryonic kidney HEK293T culture (1.25 ng/μL), gRNA (22.5 nM), and a poly U FAM reporter (125 nM). Fluorescence signals at 485 nm excitation and 525 nm

https://doi.org/10.1021/acssensors.6c00841
ACS Sens. XXXX, XXX, XXX−XXX

emission (Ex 485/Em 525 nm) were recorded every 5 min for 50 min at 37 °C (384-well microplate, SpectraMax iD5, Molecular Devices). For LwaCas13a synthetic DNA detection, reactions (20 μL) contained 3 μL of RPA products, murine RNase inhibitor (1 U/μL), NEBuffer 2.1 (1×), LwaCas13a (90 nM), HEK293T RNA (1.25 ng/μL), gRNA (45 nM), Texas Red reporter (125 nM), ribonucleotide triphosphates (rNTPs) at 1 mM each, and T7 RNA polymerase (1.5 U/μL). Fluorescence (Ex 585/Em 625 nm) was recorded every 5 min for 60 min at 37 °C. LwaCas13a SNP-specific detection in human genomic DNA (gDNA) used identical conditions with optimized Cas/gRNA ratios: CYP2C19*2 (22.5 nM/11.25 nM), *3 (90 nM/22.5 nM), and *17 (90 nM/45 nM). For LbaCas12a DNA detection, LbaCas12a (600 nM) was preincubated with gRNA (300 nM) and NEBuffer 2.1 (1×) for 10 min at 37 °C to generate a Cas-gRNA construct. The following CRISPR-based reaction (20 μL) contained 3 μL of the RPA product, a murine RNase inhibitor (1 U/μL), NEBuffer 2.1 (1×), a Cas-gRNA construct (90 nM/45 nM), and a HEX reporter (250 nM). Fluorescence (Ex 530/Em 570 nm) was measured every 5 min for 60 min at 37 °C. For multiplexed DNA detection, reactions (20 μL) contained 3 μL of the RPA product, a murine RNase inhibitor (1 U/μL), NEBuffer 2.1 (1×), LwaCas13a (90 nM), an LbaCas12a-specific Cas-gRNA construct (90 nM/45 nM), HEK293T RNA (1.25 ng/μL), LwaCas13a-specific gRNA (45 nM), a Texas Red reporter (125 nM), a HEX reporter (250 nM), rNTPs (1 mM each), and T7 RNA polymerase (1.5 U/μL). Fluorescence was recorded at Ex 585/Em 625 nm and Ex 530/Em 570 nm every 5 min for 60 min at 37 °C.

Sample Preparation

gDNA was isolated using the DNeasy Blood & Tissue Kit (Qiagen) according to the manufacturer's instructions, where aliquots were stored at −80 °C. For simplified crude extraction, 10 μL of whole human blood was mixed with 66 μL of phosphate-buffered saline and 24 μL of lysis master mix (at a final concentration of 100 mM Tris-2-carboxyethyl-phosphine, 1 mM EDTA, and 0.8 U/μL murine RNase inhibitor), incubated 5 min at 40 °C and 5 min at 95 °C, and directly used for isothermal amplification.[34] The complete assay required 140 min from sample to readout when using column-based extraction with fluorescence detection and 130 min when using simplified crude extraction with fluorescence detection. From sample to readout, the lateral-flow workflow with column-based extraction required 145 min.

Genotyping of Patient Samples

For each patient sample, PCR amplification was performed for CYP2C19*2, *3, and *17 using previously published PCR FP and RP.[35] PCR-based target amplification was performed using the Q5 High-Fidelity 2x Master Mix (NEB) according to the manufacturer's instructions with an annealing temperature of 57 °C, as calculated with the melting temperature calculator (NEB). PCR amplification of CYP2C19*2, *3, and *17 yielded products of 321, 419, and 473 nucleotides in length, respectively. PCR products were cleaned with a 1× paramagnetic bead clean-up, washed three times with 200 μL of ethanol (70%), and eluted with 15 μL of elution buffer (Qiagen).[36] Cleaned PCR products were diluted to a sample concentration of 5 ng/μL and sent for Sanger sequencing using T7P for sequencing (Eurofins Genomics). Results were analyzed through alignment with the reference sequence (Geneious Prime).

Lateral-Flow Detection Assay

The lateral-flow detection was conducted similarly to the fluorescence-based assay with modifications. For CYP2C19*2 detection, reactions (20 μL) contained 3 μL of RPA products, a murine RNase inhibitor (1 U/μL), NEBuffer 2.1 (1×), LwaCas13a (90 nM), an LbaCas12a-specific Cas-gRNA construct (180 nM/90 nM), LwaCas13a-specific gRNA (45 nM), a biotin-FAM reporter (5 nM), a digoxigenin-FAM reporter (5 nM), rNTPs (0.75 mM each), and T7 RNA polymerase (1.5 U/μL). For CYP2C19*3 detection, reactions contained 3 μL of RPA products, a murine RNase inhibitor (1 U/μL), NEBuffer 2.1 (1×), LwaCas13a (85.5 nM), an LbaCas12a-specific Cas-gRNA construct (180 nM/90 nM), LwaCas13a-specific gRNA (42.75 nM), a biotin-FAM reporter (5 nM), a digoxigenin-FAM reporter (5 nM), rNTPs (1 mM each), and T7 RNA polymerase (1.5 U/μL). CRISPR-based reactions (20 μL) were performed on a heat block at 37 °C for 1 h and then combined with a Hybridetect Assay buffer (80 μL). Subsequently, lateral-flow sticks (Hybridetect 2 T, Milenia Biotec) were inserted and incubated at room temperature for 5 min for CYP2C19*2 and 15 min for CYP2C19*3 before imaging.

Patient Populations and Ethics

In total, 110 samples from study participants were collected from multiple sites. To enable analytical validation across all genotype classes, the cohort was intentionally enriched for CYP2C19*3 carriers, reflecting the low population frequency of this allele. Human gDNA samples from the biobank of the Department of Neurology at the Technical University of Munich, School of Medicine, Klinikum rechts der Isar, were subjected to whole-exome sequencing at the Regeneron Genetics Center (New York, USA; ethics approval number: 308/17S). Generated sequences had a 20-fold coverage in >80% of target bases, and subsequent quality control was based on the contamination score (contamination <5% via verifyBamID software & HET/MUT ratio), sample duplication, gender concordance, and exome-genotype concordance. Additional samples were obtained from discarded material from adults (>18 years) presenting to Massachusetts General Hospital. Whole human blood samples were frozen at −80 °C before research use. The study was granted exemption from informed consent due to the use of anonymized discarded clinical samples and was approved by the Mass General Brigham IRB, Protocol no. 2022P000747. Additional human blood samples from Taiwan were collected from individuals after obtaining informed consent, with approval from the Institutional Review Board of KMUH (KMUHIRB-G(II)–20160024). Human blood samples were employed for gDNA isolation and CYP2C19 genotyping. The isolated gDNA was frozen at −80 °C and stored for research purposes.

Statistical Analysis

The mean relative fluorescence unit value of CRISPR-Cas-based reactions was calculated based on four independent reactions and presented as mean ± standard deviation, unless indicated otherwise. Statistical significance was assessed using unpaired *t*-tests, with false discovery rate control using the two-stage step-up method of Benjamini, Krieger, and Yekutieli, comparing WT/HET and HET/MUT targets, unless specified otherwise. Statistical annotations were shown only for statistically significant differences, $P < 0.05$ (*), $P < 0.01$ (**), $P < 0.001$ (***), and $P < 0.0001$ (****). Genotyping accuracy was calculated as the proportion of correctly classified samples among all samples tested. Discriminatory power was calculated per enzyme. For LwaCas13a, it was defined by MUT/HET and MUT/WT fluorescence ratios, whereas for LbaCas12a, it was defined by WT/MUT ratios. The genotyping score was calculated by dividing the area under the curve (AUC) of each patient sample by the AUC of the synthetic standard (MUT for LwaCas13a and WT for LbaCas12a) between 30 and 60 min using the following equation: $\text{Genotyping score} = \frac{\int_{30}^{60} f(\text{sample})}{\int_{30}^{60} f(\text{positive control})}$. The genotyping ratio was calculated by dividing the genotyping score of HEX by the genotyping score of Texas Red for each sample. For the one-guide system, cut-off thresholds were defined as the mean between the maximum WT and minimum HET genotyping scores, as well as between the maximum HET and minimum MUT scores. For the dual-guide system, thresholds were defined per enzyme. For LbaCas12a, the threshold was set as the mean of the maximum genotyping score from MUT and the minimum from WT and HET. For LwaCas13a, the threshold was set as the mean of the maximum genotyping score from WT and the minimum from

https://doi.org/10.1021/acssensors.6c00841
ACS Sens. XXXX, XXX, XXX–XXX

HET and MUT. Statistical analyses were performed in GraphPad Prism 8.4.3.

RESULTS AND DISCUSSION

Screening CYP2C19 gRNAs to Identify Optimal Mismatch Positions for Variant Discrimination

To enable discrimination of WT, HET, and MUT CYP2C19 variants, we systematically explored the impact of the SNP position of the gRNA in relation to its target. We tested LwaCas13a gRNAs that were fully complementary to the variant sequence ("MUT-sensing"), but differed from the WT sequence at one single nucleotide (the SNP) located at positions 1 to 12 within the spacer region, counted from the 5′ to 3′ end of the gRNA. Using a fluorescence-based CRISPR assay, in which LwaCas13a cleaves a quenched reporter upon target RNA recognition (Figures 1b), we tested synthetic RNA targets representing CYP2C19 WT and MUT sequences and generated the HET target by mixing WT and MUT RNA targets at a 1:1 ratio. As expected, we consistently observed higher fluorescence signals for MUT targets compared to WT (Figures 1c–e and S1–S3). However, only few gRNAs generated fluorescence signals for HET targets that enabled a clear differentiation from both WT and MUT. We found that the position of the SNP within the spacer markedly influenced the gRNA's ability to discriminate between WT, HET, and MUT targets based on their fluorescence signals, but it did not exhibit a consistent 5′-bias as previously reported.[31−33] By scoring gRNAs based on their MUT/HET and MUT/WT ratios (Table S1), we identified those with the highest discriminatory power. For further analyses, we selected the gRNA with a mismatch at position 2 for CYP2C19*2 (gRNA 2-2, Figures 1c, S1, Tables S1, S2), at position 12 for *3 (gRNA 3-12, Figures 1d, S2, Tables S1, S2), and at positions 7, 9, or 12 for *17 (gRNAs 17-7, 17-9, 17-12, Figures 1e, S3, Tables S1, S2). Notably, the optimal mismatch position differed among the three targets, indicating that discrimination capacity is influenced not only by the mismatch location but also by the surrounding sequence context.

We then tested the selected gRNAs on synthetic DNA targets, mimicking human gDNA, using a modified SHERLOCK protocol.[31−33] This included isothermal RPA, T7-driven RNA transcription, and target detection via MUT-sensing LwaCas13a guided by the selected gRNAs (2-2, 3-12, 17-7, 17-9, and 17-12; Figure 2). Surprisingly, the discriminative power observed with synthetic DNA targets did not fully reproduce our previous findings with RNA targets. Only gRNA 3-12 achieved high discrimination based on MUT/HET and MUT/WT fluorescence ratios, whereas gRNAs 2-2, 17-7, 17-9, and 17-12 exhibited low discriminatory power (Figure 2a, Tables S3, S4). Therefore, we selected gRNA 3-12 for CYP2C19*3 genotyping and proceeded to further optimize gRNAs for *2 and *17. Next, we hypothesized that introducing additional synthetic mismatches in these gRNAs could further improve their target specificity, as previously demonstrated in SHERLOCK assays.[31−33] Mismatches were placed either to the left (L), to the right (R), or on both sides of the SNP position (LR). This resulted in gRNAs with two mismatches to the WT and one to the MUT sequence (left or right design) or three mismatches to the WT and two to the MUT sequence (left-right design) (Figure 2b).

We observed that for CYP2C19*2, introducing additional mismatches further enhanced discriminatory power, with gRNA 2-2-L achieving the highest MUT/HET and MUT/WT fluorescence ratios (Figure 2c, left, Table S3). For CYP2C19*17, the design with two additional mismatches (gRNA 17-9-LR) showed the best performance (Figure 2c, right, Table S3). Both modified gRNAs outperformed their original counterparts that lacked synthetic mismatches, showing that the introduction of synthetic mismatches adjacent to the SNP can improve gRNA specificity, in line with prior studies.[31−33] Interestingly, we did not observe a consistent pattern regarding how additional synthetic mismatches influence target specificity. Moreover, introducing two additional mismatches did not reduce overall signal intensity, suggesting mismatch tolerance in target detection and underscoring the need for experimental gRNA validation. Our finding may offer a simple and transferable optimization strategy for other pharmacogenetic targets, informing broader CRISPR diagnostics development. Based on these results, gRNAs 2-2-L, 3-12, and 17-9-LR were selected for the final CRISPR-Cas-based CYP2C19 genotyping assay.

Next, we evaluated whether the optimized assay could genotype CYP2C19 variants directly from human gDNA. Fluorescence signal intensity was used to classify genotypes: low for WT, intermediate for HET, and high for MUT samples (Figure 3a). To account for day-to-day variability in signal intensity, synthetic MUT DNA targets were included alongside each run. Based on normalized fluorescence signals, which we used to calculate a genotyping score for each sample, the assay achieved genotyping accuracies of 100% for CYP2C19*2 (Figure 3b), 88.2% for *3 (Figure 3c), and 100% for *17 (Figure 3d), relative to Sanger sequencing. However, the one-guide system is inherently limited for HET/MUT discrimination after RPA, because HET samples contain only one mutant allele and therefore differ from MUT samples mainly in mutant target abundance. This quantitative difference can be obscured by RPA's inherent amplification variability, making classification with a single MUT-sensing reporter less robust.

Multiplexed CRISPR-Based CYP2C19 Genotyping Assay with Enhanced Accuracy

To enhance the robustness of our genotyping assay and to further improve the differentiation of CYP2C19*3, we investigated whether incorporating a second Cas enzyme, LbaCas12a, sensing the WT allele could enhance the assay's genotyping accuracy (Figure 3e, left). In this multiplexed assay, the collateral cleavage of each enzyme was simultaneously measured using two distinct reporter molecules, with a HEX carrying DNA oligo reporting on LbaCas12a activity and a Texas Red carrying RNA oligo reporting on LwaCas13a activity. This approach eliminates the need for LwaCas13a to distinguish between HET and MUT samples. In the multiplexed setup, LwaCas13a produces high Texas Red signals for both HET and MUT samples but low signals for WT, whereas LbaCas12a produces high HEX signals for both WT and HET samples but low signals for MUT samples (Figure 3e, right). The two readouts combined yield a unique signal pattern for each genotype (WT = low Texas Red and high HEX; HET = high Texas Red and high HEX; MUT = high Texas Red and low HEX). Unlike LwaCas13a, LbaCas12a requires a protospacer adjacent motif (PAM) for target recognition and cleavage. As LbaCas12a has been reported to recognize several

https://doi.org/10.1021/acssensors.6c00841
ACS Sens. XXXX, XXX, XXX−XXX

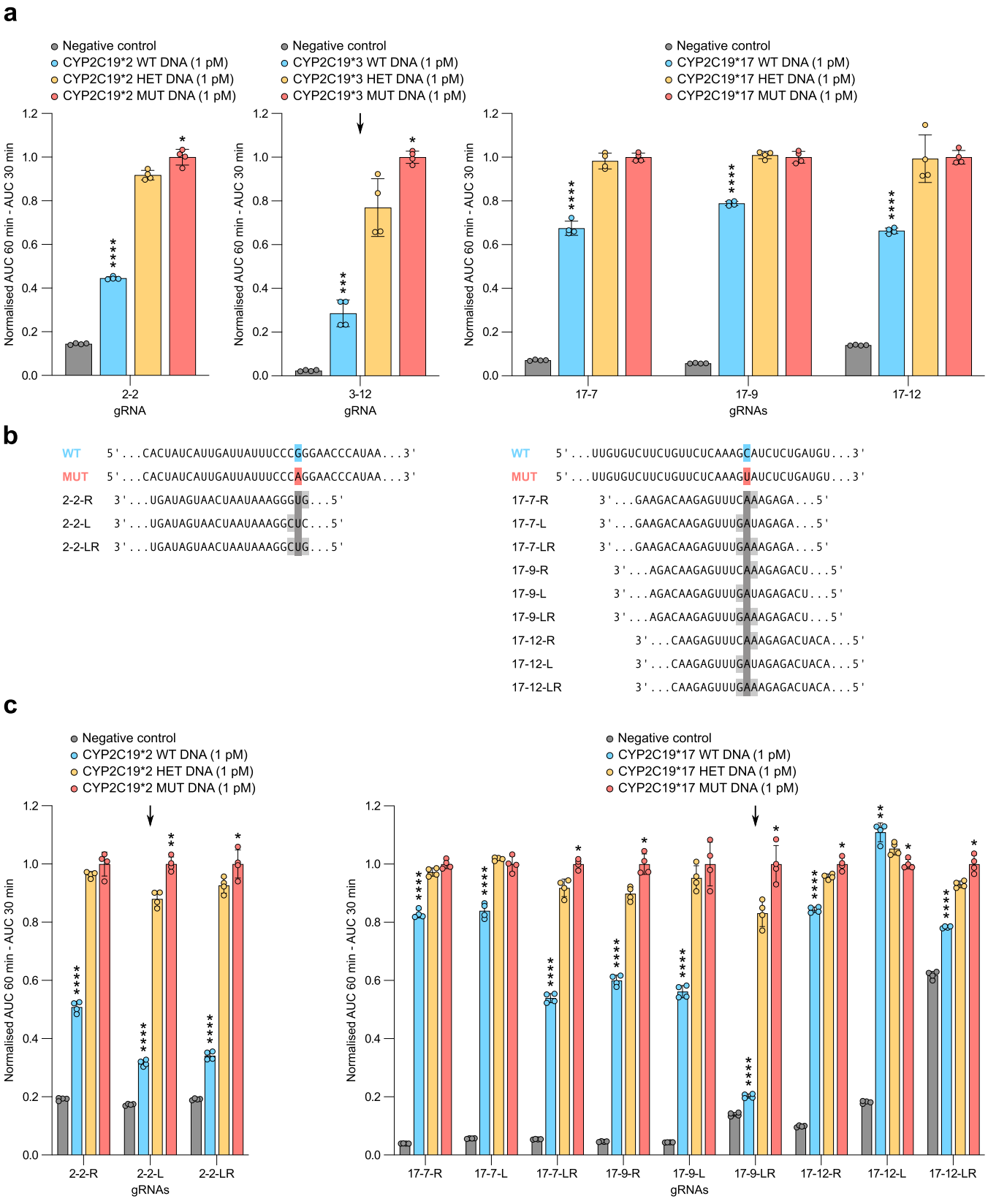

Figure 2. Systematic gRNA screen for CYP2C19 genotyping on synthetic DNA targets. (a) Bar graphs showing the fluorescence signal of the selected gRNAs (2-2, 3-12, 17-7, 17-9, 17-12) for CYP2C19*2 (left), *3 (middle), and *17 (right). (b) Design of gRNAs for CYP2C19*2 (left) and *17 (right). Synthetic mismatches, highlighted in light gray, are introduced into the spacer of gRNAs for CYP2C19*2 and gRNAs 17-7, 17-9, and 17-12 for CYP2C19*17. (c) Bar graphs showing the fluorescence signal of the gRNAs with synthetic mismatches for CYP2C19*2 (left) and *17 (right). (a, c) $n = 4$ independent replicates. Synthetic DNA targets at 1 pM. Bar graphs indicate mean ± SD. $P < 0.05$ (*), $P < 0.01$ (**), $P < 0.001$ (***), and $P < 0.0001$ (****). Selected final gRNAs are indicated by solid arrows.

https://doi.org/10.1021/acssensors.6c00841
ACS Sens. XXXX, XXX, XXX−XXX

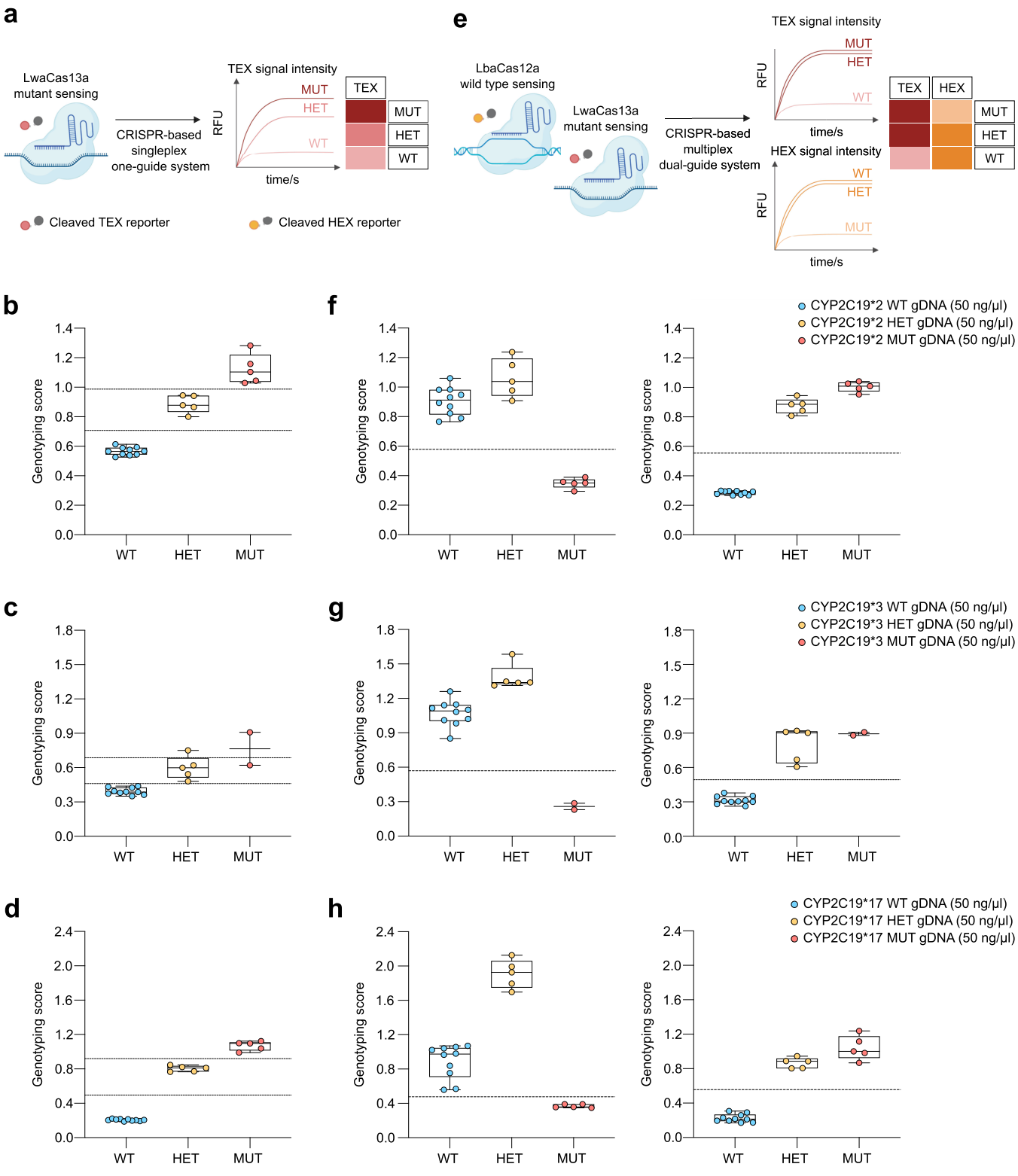

Figure 3. Comparison of one-guide and dual-guide genotyping systems on human gDNA samples. (a, e) Schematic illustrations of the one-guide (a) and dual-guide (e) CRISPR-based systems. (a) One-guide system utilizes only one gRNA, which is optimized for LwaCas13a. It cleaves Texas Red (TEX) in the presence of a MUT sample. This yields low, medium, or high fluorescence signals corresponding to WT, HET, or MUT, respectively. (e) Dual-guide system uses two gRNAs, one for LwaCas13a and one for LbaCas12a. The former cleaves Texas Red in the presence of a MUT sample, whereas the latter cleaves HEX in the presence of a WT sample. A WT yields a high LbaCas12a but a low LwaCas13a signal. A HET yields a high fluorescence signal in both, whereas a MUT yields a low LbaCas12a but a high LwaCas13a signal. (b–d, f–h) Box plots showing genotyping scores for human gDNA samples at 50 ng/μL for CYP2C19*2 (b, f), *3 (c, g), and *17 (d, h) using the one-guide system (b, c, d) and dual-guide system (f, g, h). For the dual-guide system, LbaCas12a is illustrated on the left and LwaCas13a on the right. Patient genotypes are on the *x*-axis, and genotyping scores on the *y*-axis, with blue representing WT, orange for HET, and red for MUT samples. Genotyping scores were

https://doi.org/10.1021/acssensors.6c00841
ACS Sens. XXXX, XXX, XXX–XXX

Figure 3. continued

calculated as the ratio of the area under the fluorescence curve of each sample to that of the corresponding synthetic positive control, as described in the Statistical Analysis section. Dashed lines indicate the genotyping cut-off thresholds separating WT, HET, and MUT classifications, which were defined based on the distribution of genotyping scores for each group, as described in the Statistical Analysis section. Data points represent the mean of 3 independent replicates, with each point corresponding to a different patient. Box plots indicate the median and interquartile range. Whiskers indicate the minimum and maximum values.

non-canonical PAMs in addition to its canonical TTTV PAM,[37,38] we designed and evaluated CYP2C19 WT-sensing gRNAs adjacent to either canonical or non-canonical PAMs (Figure S4). Among those, we selected the gRNAs with the highest WT/MUT fluorescence ratios (Tables S5, S6), namely, gRNA 2-3-1 for CYP2C19*2, 3-5-3 for *3, and 17-5-4 for *17.

Next, we multiplexed LwaCas13a (MUT-sensing gRNAs 2-2-L, 3-12, 17-9-LR) with LbaCas12a (WT-sensing gRNAs 2-3-1, 3-5-3, 17-5-4) and tested them on the same pre-amplified patient samples as in the one-guide assay, ensuring a direct comparison between both approaches. The dual-guide assay achieved genotyping accuracies of 100% for CYP2C19*2 (Figure 3f), 100% for *3 (Figure 3g), and 100% for *17 (Figure 3h). This systematic comparison demonstrates that both approaches achieved high genotyping accuracy, with the single-guide system enabling differentiation between WT, HET, and MUT genotypes in a single reaction, streamlining assay setup and minimizing reagent use. Nonetheless, the dual-guide system, combining LwaCas13a and LbaCas12a, further improved HET discrimination by leveraging their orthogonal cleavage preferences, making it especially valuable for clinical applications requiring robust genotype distinction.

Assessment of CYP2C19 Genotyping in a Patient Cohort

To further evaluate the genotyping accuracy of the optimized dual-guide approach, we genotyped a multicenter human cohort of 110 participants from the USA, Germany, and Taiwan, each participant contributing one gDNA sample, thereby capturing all common CYP2C19 metabolizer phenotypes. For this analysis, we utilized a simplified genotyping ratio that generated one single value per sample to streamline data interpretation. The genotyping ratio was calculated as the ratio of the HEX signal (LbaCas12a, WT-sensing) to the Texas Red signal (LwaCas13a, MUT-sensing), such that the highest genotyping ratios corresponded to WT samples, intermediate ratios to HET samples, and the lowest ratios to MUT samples (Figure 4a). We next compared the genotyping ratios with the current clinical gold standard, PCR, followed by Sanger sequencing. Since fluorescence signals and genotyping ratios differed among the three CYP2C19 variants, most likely due to sequence-dependent gRNA and Cas enzyme activities, we adjusted the cutoffs between the genotype groups (WT, HET, MUT) individually for each variant. Using the adjusted cutoffs, we achieved a genotyping accuracy of 97.3% for CYP2C19*2 (Figure 4b), 100.0% for *3 (Figure 4c), and 99.1% for *17 (Figure 4d).

Point-of-Care Genotyping via Crude DNA Extraction and Multi-Analyte Lateral-Flow Readout

To enable point-of-care genotyping, we optimized a lateral-flow assay for CYP2C19*2 and *3 as both variants are associated with reduced CYP2C19 activity, representing the main risk factors for adverse outcomes.[2,39,40] We focused on the loss-of-function alleles CYP2C19*2 and *3, as these are the variants currently actionable for clopidogrel therapy and mandatory for mavacamten genotyping. While CYP2C19*17 was not included in this proof of concept, the dual-guide setup is in principle compatible with lateral-flow detection and could be extended to *17 in future work.[2,40] This strategy is consistent with existing genotyping assays and current clinical recommendations.[10,11]

For simultaneous detection of WT, HET, and MUT genotypes for either CYP2C19*2 or *3 in a single reaction, we developed a multi-analyte lateral-flow assay with three test bands consisting of streptavidin (test band T2), anti-digoxigenin (test band T1), and anti-conjugate (control band C) antibodies (Figure 5a). The multiplexed CRISPR-based assay combines MUT-sensing LwaCas13a and WT-sensing LbaCas12a, which, upon target recognition, cleave RNA reporter oligos carrying 3'-biotin or DNA reporter oligos carrying 3'-digoxigenin, respectively. Both reporter oligos carry a 5′FAM, which binds anti-FAM gold nanoparticles (AuNPs). For WT samples, activated LbaCas12a cleaves digoxigenin-labeled reporters, preventing their capture at the T1 test band, while intact biotin-labeled reporters are captured at the T2 test band. For HET samples, activated LwaCas13a and LbaCas12a cleave both reporters, preventing formation of both test bands. For MUT samples, activated LwaCas13a cleaves biotin-labeled reporters, preventing their capture at the T2 test band, while intact digoxigenin-labeled reporters are captured at the T1 test band. In all cases, anti-FAM AuNPs migrate to the control band C, where anti-conjugate antibodies capture them, confirming proper assay flow.

We next evaluated the assay's ability to genotype CYP2C19*2 and *3 using a multi-analyte lateral-flow readout with one stick per variant, combining isothermal amplification of human gDNA with multiplexed CRISPR-based detection. We observed three distinct signal patterns (Figure 5b): On each variant specific strip, samples that were WT for the corresponding SNP showed the absence of the T1 test band, samples that were HET for that SNP lacked both test bands, and samples that were MUT for that SNP showed the absence of the T2 test band. Each genotype yielded a unique, visually interpretable band pattern, enabling unambiguous identification without the need for instrumentation.

To streamline the workflow and further optimize for rapid isothermal genotyping at the point of care, we assessed whether a simplified crude DNA extraction protocol, circumventing the need for column-based DNA isolation, would be compatible with CRISPR-based CYP2C19 genotyping (Figure 5c). In this protocol, human blood samples were incubated at 40 °C for 5 min, followed by 95 °C for 5 min. The protocol was followed by isothermal amplification using RPA at 39 °C for 60 min and multiplexed CRISPR detection at 37 °C for 60 min.

To test the simplified crude extraction protocol, we used a fluorescence-based readout for quantitative assessment of the

https://doi.org/10.1021/acssensors.6c00841
ACS Sens. XXXX, XXX, XXX−XXX

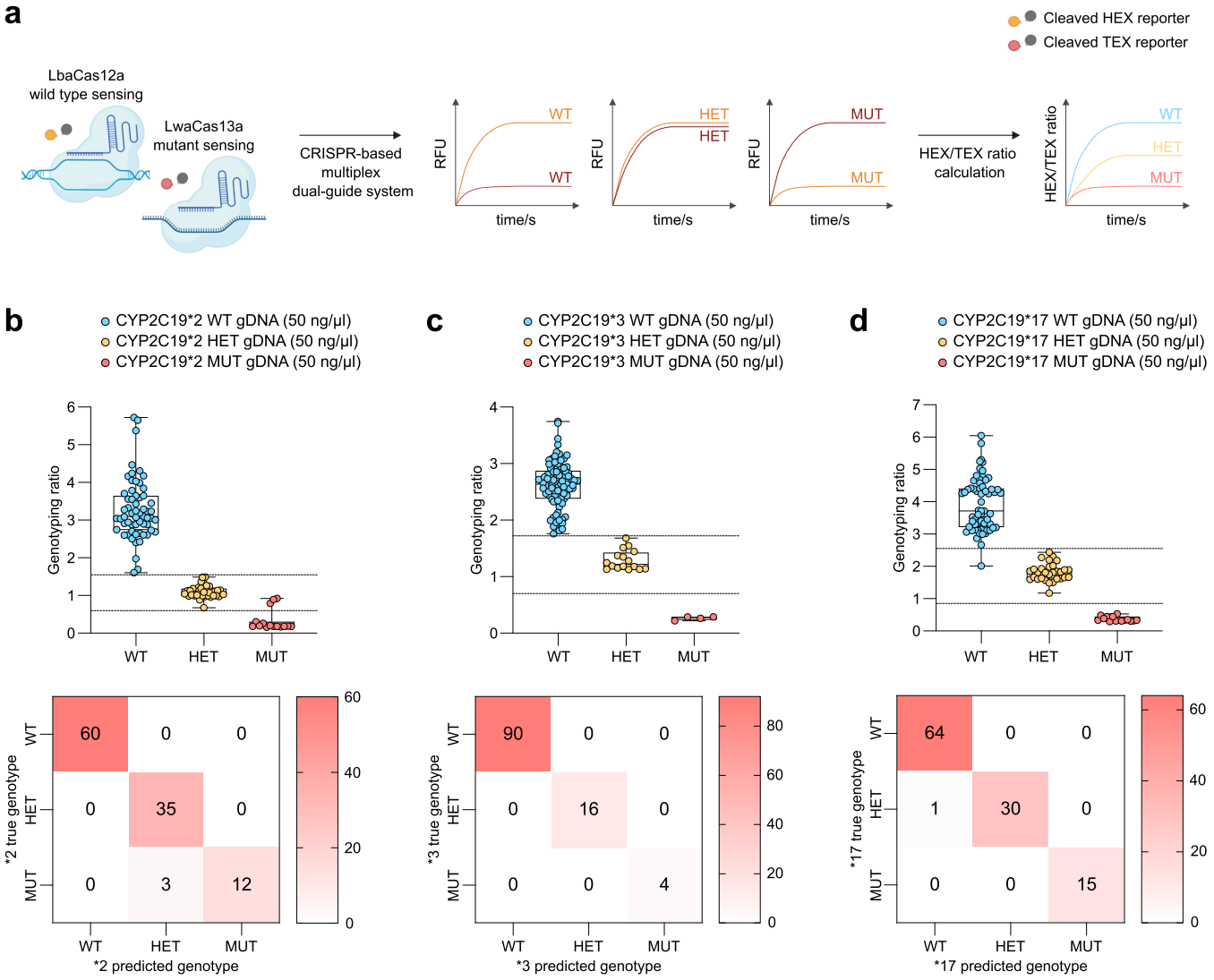

Figure 4. CRISPR-based CYP2C19 genotyping in a multiethnic, multicenter patient cohort. (a) Illustration of data processing used for genotype classification in panels (b–d). The dual-guide system multiplexes LbaCas12a (HEX) and LwaCas13a (Texas Red), generating two fluorescence signals per sample corresponding to WT (left), HET (middle), or MUT (right) genotypes. The genotyping ratio is calculated by dividing the genotyping score of HEX by the genotyping score of Texas Red for each sample, enabling simplified classification based on a single derived value. TEX, Texas Red. (b–d) Box plots (top) and confusion matrix (bottom) showing CRISPR-based genotype prediction for 110 samples from study participants collected from the USA, Germany, and Taiwan. gDNA samples at 50 ng/µL were genotyped with the CRISPR-based assay for CYP2C19*2 (b), *3 (c), and *17 (d). Top: Data points represent the mean of 3 independent replicates, with each point corresponding to a different patient. Box plots indicate the median and interquartile range. Whiskers indicate the minimum and maximum values. Dashed lines indicate the genotyping cut-off thresholds separating WT, HET, and MUT classifications, which were defined individually for each variant. Bottom: Accuracy of the CRISPR-based assay compared with Sanger sequencing, the current gold standard. The alignment of the true and predicted genotypes indicates correct classification.

assay's discriminatory power. As illustrated for CYP2C19*2, the simplified crude extraction protocol (Figure 5d) enabled accurate genotype classification. WT samples showed high LbaCas12a (1.00) but low LwaCas13a scores (0.28), HET samples showed high scores for both enzymes (1.24 and 1.20), and MUT samples showed the opposite pattern (0.45 and 1.00). Crude extraction was demonstrated here for CYP2C19*2; clinical validation will require its extension to *3, as well as to a broader range of sample types and operators, in future studies. The results indicate that crude extraction is compatible with CRISPR-based detection while eliminating the need for column-based gDNA extraction and purification. The combination of simplified sample preparation, isothermal amplification, multiplexed CRISPR-based detection, and multianalyte lateral-flow readout enables CYP2C19 genotyping suitable for point-of-care use.

■ CONCLUSIONS

In conclusion, we developed a rapid, accurate, low-complexity CRISPR-based assay for CYP2C19 genotyping that combines isothermal amplification, dual-guide detection, and simplified sample preparation with fluorescence or lateral-flow readout, enabling point-of-care testing. Its diagnostic

https://doi.org/10.1021/acssensors.6c00841
ACS Sens. XXXX, XXX, XXX–XXX

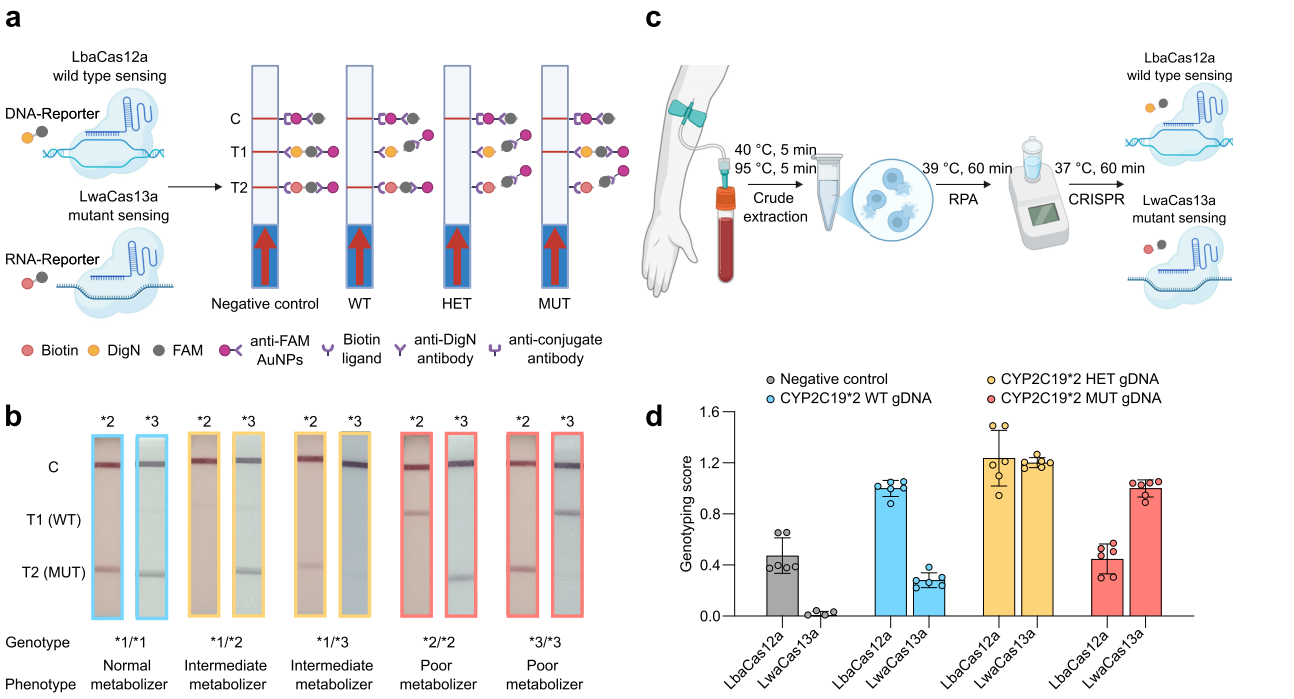

Figure 5. Multi-analyte lateral-flow readout of the multiplexed CRISPR-based assay on human gDNA and crude extraction protocol using human blood samples. (a) Schematic illustration of the multi-analyte lateral-flow assay using multiplexed CRISPR detection for CYP2C19 genotyping. The system employs LbaCas12a and LwaCas13a for simultaneous DNA and RNA detection on a single test strip containing three bands: control (C), WT (T1), and MUT (T2). Target-induced Cas activation cleaves the corresponding reporter, thereby preventing formation of the respective test band upon target recognition. From left to right: Lateral-flow illustrations of a negative control, WT, HET, and MUT sample. (b) Lateral-flow readouts of human gDNA samples (50 ng/μL) preamplified by RPA and applied to multiplexed CRISPR-based CYP2C19*2 (left strip) and *3 (right strip) assays. WT, HET, and MUT genotypes are indicated in blue, orange, and red, respectively. (c) Schematic illustration of the CRISPR-based CYP2C19 genotyping assay using crude extraction. Human blood samples are processed using a simplified crude extraction protocol, followed by RPA preamplification. The resulting RPA products undergo a multiplexed CRISPR-based reaction for genotype determination. (d) Bar graphs showing fluorescence signals from the multiplexed CRISPR-based CYP2C19*2 genotyping assay using products prepared with simplified crude extraction. $n = 6$ independent replicates.

performance in a multiethnic clinical cohort underscores its potential to support broader clinical implementation of pharmacogenetic testing for CYP2C19-guided therapy.

While our CRISPR-based assay is modular and adaptable to other pharmacogenetic targets, gRNA performance remains target-dependent. Sequence context, mismatch tolerance, and secondary structure may influence detection efficiency, necessitating empirical optimization for each new SNP. Although we observed high concordance with clinical gold standards, further validation in real-world clinical settings with predefined thresholds is warranted to confirm robustness. In practice, implementation may occur as near-patient testing in catheterization laboratories or cardiology wards, or as a rapid in-house assay in the local hospital laboratory, leveraging existing molecular expertise and avoiding shipment to external reference centers. Looking ahead, integrating sample preparation, amplification, and detection into a single-pot reaction represents a key goal to simplify workflows and facilitate implementation.

■ ASSOCIATED CONTENT

Supporting Information

The Supporting Information is available free of charge at https://pubs.acs.org/doi/10.1021/acssensors.6c00841.

Raw fluorescence data for systematic LwaCas13a gRNA screen for CYP2C19*2 on synthetic RNA targets (Figure S1); raw fluorescence data for systematic LwaCas13a gRNA screen for CYP2C19*3 on synthetic RNA targets (Figure S2); raw fluorescence data for systematic LwaCas13a gRNA screen for CYP2C19*17 on synthetic RNA targets (Figure S3); systematic LbaCas12a gRNA screen for CYP2C19 genotyping (Figure S4); CRISPR-based CYP2C19 genotyping in a patient cohort using the dual-guide system, with the signals from LbaCas12a and LwaCas13a shown separately (Figure S5); LwaCas13a gRNA screen on RNA: MUT/HET and MUT/WT ratios (Table S1); LwaCas13a gRNA screen on RNA: genotype comparison statistics (Table S2); LwaCas13a gRNA screen on T7-transcribed DNA: MUT/HET and MUT/WT ratios (Table S3); LwaCas13a gRNA screen on T7-transcribed DNA: genotype comparison statistics (Table S4); LbaCas12a gRNA screen: WT/MUT ratios (Table S5); LbaCas12a gRNA screen: genotype comparison statistics (Table S6); genotyping scores for simplified crude extraction (Table S7); RPA and PCR primer sequences (Table S8); gRNA sequences for LwaCas13a gRNA screen (Table S9); gRNA sequences for LbaCas12a gRNA screen (Table S10); synthetic WT and MUT target sequences

https://doi.org/10.1021/acssensors.6c00841
ACS Sens. XXXX, XXX, XXX−XXX

(Table S11); and reporter sequences and fluorophores (Table S12) (PDF)

AUTHOR INFORMATION

Corresponding Author

Michael M. Kaminski – *Berlin Institute for Medical Systems Biology, Max Delbrück Center for Molecular Medicine in the Helmholtz Association, Berlin 10115, Germany; Department of Nephrology and Medical Intensive Care, Charité - Universitätsmedizin Berlin, Berlin 10117, Germany; Berlin Institute of Health, Berlin 10117, Germany;* orcid.org/0000-0003-0429-7027;
Email: michael.kaminski@charite.de

Authors

Alexander J. Schubert – *Berlin Institute for Medical Systems Biology, Max Delbrück Center for Molecular Medicine in the Helmholtz Association, Berlin 10115, Germany; Department of Nephrology and Medical Intensive Care, Charité - Universitätsmedizin Berlin, Berlin 10117, Germany; Berlin Institute of Health, Berlin 10117, Germany;* orcid.org/0000-0002-6907-5276

Qiyao Meng – *Berlin Institute for Medical Systems Biology, Max Delbrück Center for Molecular Medicine in the Helmholtz Association, Berlin 10115, Germany; Department of Nephrology and Medical Intensive Care, Charité - Universitätsmedizin Berlin, Berlin 10117, Germany*

Joshua Hoffmann – *Berlin Institute for Medical Systems Biology, Max Delbrück Center for Molecular Medicine in the Helmholtz Association, Berlin 10115, Germany; Department of Nephrology and Medical Intensive Care, Charité - Universitätsmedizin Berlin, Berlin 10117, Germany*

Josefine Rau – *Berlin Institute for Medical Systems Biology, Max Delbrück Center for Molecular Medicine in the Helmholtz Association, Berlin 10115, Germany*

Fabian Abele – *Berlin Institute for Medical Systems Biology, Max Delbrück Center for Molecular Medicine in the Helmholtz Association, Berlin 10115, Germany; Department of Nephrology and Medical Intensive Care, Charité - Universitätsmedizin Berlin, Berlin 10117, Germany*

Robert Greensmith – *Berlin Institute for Medical Systems Biology, Max Delbrück Center for Molecular Medicine in the Helmholtz Association, Berlin 10115, Germany; Department of Nephrology and Medical Intensive Care, Charité - Universitätsmedizin Berlin, Berlin 10117, Germany*

Carlos Cordero – *Berlin Institute for Medical Systems Biology, Max Delbrück Center for Molecular Medicine in the Helmholtz Association, Berlin 10115, Germany; Department of Nephrology and Medical Intensive Care, Charité - Universitätsmedizin Berlin, Berlin 10117, Germany*

Antonia Ibel – *Berlin Institute for Medical Systems Biology, Max Delbrück Center for Molecular Medicine in the Helmholtz Association, Berlin 10115, Germany; Department of Nephrology and Medical Intensive Care, Charité - Universitätsmedizin Berlin, Berlin 10117, Germany*

Julia M. Mandler – *School of Medicine and Health, Klinikum rechts der Isar, Department of Neurology, Technical University of Munich, Munich 81675, Germany*

Kai-Uwe Eckardt – *Department of Nephrology and Medical Intensive Care, Charité - Universitätsmedizin Berlin, Berlin 10117, Germany*

Jan Halbritter – *Department of Nephrology and Medical Intensive Care, Charité - Universitätsmedizin Berlin, Berlin 10117, Germany; Renal Division, Department of Medicine, Faculty of Medicine and Medical Center - University of Freiburg, Freiburg 79106, Germany*

Anand S. Dighe – *Harvard Medical School, Boston, Massachusetts 02115, United States; Department of Pathology, Massachusetts General Hospital, Boston, Massachusetts 02114, United States*

Xiao Tan – *Harvard Medical School, Boston, Massachusetts 02115, United States; Wyss Institute for Biologically Inspired Engineering, Harvard University, Boston, Massachusetts 02115, United States; Division of Gastroenterology, Massachusetts General Hospital, Boston, Massachusetts 02114, United States; Institute for Medical Engineering and Science, Department of Biological Engineering, Massachusetts Institute of Technology, Cambridge, Massachusetts 02139, United States*

Daw-Yang Hwang – *National Institute of Cancer Research, National Health Research Institutes, Tainan 704, Taiwan; Division of Nephrology, Department of Medicine, Kaohsiung Medical University Hospital, Kaohsiung Medical University, Kaohsiung 807, Taiwan*

Tobias Petzold – *Department of Cardiology, Angiology and Intensive Care Medicine, Deutsches Herzzentrum der Charité, University Hospital Berlin, Campus Benjamin Franklin, Berlin 12203, Germany; DZHK (German Centre for Cardiovascular Research), Partner Site Berlin, Berlin 10785, Germany; Friede Springer Center for Cardiovascular Prevention, Charité - Universitätsmedizin Berlin, Berlin 12203, Germany*

Philipp Enghard – *Department of Nephrology and Medical Intensive Care, Charité - Universitätsmedizin Berlin, Berlin 10117, Germany; German Rheumatism Research Center Berlin (DRFZ), An Institute of the Leibniz Foundation, Berlin 10117, Germany*

Complete contact information is available at: https://pubs.acs.org/doi/10.1021/acssensors.6c00841

Author Contributions

[†]A.J.S. and Q.M. contributed equally to this work. A.J.S., Q.M., and M.M.K. were responsible for the study design, while A.J.S. and Q.M. developed and validated the CYP2C19 genotyping assay. J.H. assisted in the validation of the CYP2C19 genotyping assay and optimization of the lateral-flow assay. J.R., F.A., and C.C. assisted in the optimization of the crude extraction protocol. The design and analysis of experiments were supported by R.G., A.I., K.U.E., J.P.H., T.P., and P.E., and clinical samples were provided by J.M.M., A.S.D., X.T., and D.Y.H. All authors participated in the manuscript writing.

Notes

The authors declare no competing financial interest.

ACKNOWLEDGMENTS

M.M.K. received funding from the German Research Foundation's Emmy Noether Program (grant no. KA5060/1-1) and also took part in the Clinician Scientist Program, which

https://doi.org/10.1021/acssensors.6c00841
ACS Sens. XXXX, XXX, XXX–XXX

is supported by Charité - Universitätsmedizin Berlin and the Berlin Institute of Health (BIH). A.J.S. was a recipient of the BIH Medical Doctor Research Stipend. J.P.H. received funding from the German Research Foundation's Heisenberg Program (grant no. HA 6908/4-1). X.T. received funding from the NIH NIDDK (5K08DK132516). T.P. received funding from the German Research Foundation's Heisenberg Program (grant no. PE 2704/4-1, PE2704/5-1) and DZHK (German Centre for Cardiovascular Research; BHF-81X2100286, 81X2100293). We extend our gratitude to Anja Schütz and the Protein Production & Characterization Technology Platform of the Max Delbrück Center for Molecular Medicine in the Helmholtz Association, Berlin, Germany (https://www.mdc-berlin.de/protein-production-characterization), for producing the LwaCas13a protein. We would also like to acknowledge the Regeneron Genetics Center (New York, USA) for whole-exome sequencing of the gDNA samples provided by the biobank of the Department of Neurology at the Technical University of Munich (led by Prof. Dr. Bernhard Hemmer). Portions of the text were refined for clarity and grammar using an artificial intelligence language model (OpenAI GPT-5). All outputs were reviewed and edited by the authors, who take full responsibility for the content.

REFERENCES

(1) Relling, M. V.; Evans, W. E. Pharmacogenomics in the Clinic. *Nature* **2015**, *526* (7573), 343–350.

(2) Lee, C. R.; Luzum, J. A.; Sangkuhl, K.; Gammal, R. S.; Sabatine, M. S.; Stein, C. M.; Kisor, D. F.; Limdi, N. A.; Lee, Y. M.; Scott, S. A.; Hulot, J.; Roden, D. M.; Gaedigk, A.; Caudle, K. E.; Klein, T. E.; Johnson, J. A.; Shuldiner, A. R. Clinical Pharmacogenetics Implementation Consortium Guideline for CYP2C19 Genotype and Clopidogrel Therapy: 2022 Update. *Clin. Pharmacol. Ther.* **2022**, *112* (5), 959–967.

(3) Ionova, Y.; Ashenhurst, J.; Zhan, J.; Nhan, H.; Kosinski, C.; Tamraz, B.; Chubb, A. CYP2C19 Allele Frequencies in Over 2.2 Million Direct-to-Consumer Genetics Research Participants and the Potential Implication for Prescriptions in a Large Health System. *Clin. Transl. Sci.* **2020**, *13* (6), 1298–1306.

(4) Ellithi, M.; Baye, J.; Wilke, R. A. CYP2C19 Genotype-Guided Antiplatelet Therapy: Promises and Pitfalls. *Pharmacogenomics* **2020**, *21* (12), 889–897.

(5) Pereira, N. L.; Cresci, S.; Angiolillo, D. J.; Batchelor, W.; Capers, Q.; Cavallari, L. H.; Leifer, D.; Luzum, J. A.; Roden, D. M.; Stellos, K.; Turrise, S. L.; Tuteja, S.; on behalf of the American Heart Association Professional/Public Education and Publications Committee of the Council on Genomic and Precision Medicine; Council on Arteriosclerosis, Thrombosis and Vascular Biology; Council on Cardiovascular and Stroke Nursing; Council on Clinical Cardiology; Council on Peripheral Vascular Disease; and Stroke Council CYP2C19 Genetic Testing for Oral P2Y12 Inhibitor Therapy: A Scientific Statement From the American Heart Association. *Circulation* **2024**, *150* (6).

(6) Mega, J. L.; Close, S. L.; Wiviott, S. D.; Shen, L.; Hockett, R. D.; Brandt, J. T.; Walker, J. R.; Antman, E. M.; Macias, W.; Braunwald, E.; Sabatine, M. S. Cytochrome P-450 Polymorphisms and Response to Clopidogrel. *N. Engl. J. Med.* **2009**, *360* (4), 354–362.

(7) Collet, J.-P.; Hulot, J.-S.; Pena, A.; Villard, E.; Esteve, J.-B.; Silvain, J.; Payot, L.; Brugier, D.; Cayla, G.; Beygui, F.; Bensimon, G.; Funck-Brentano, C.; Montalescot, G. Cytochrome P450 2C19 Polymorphism in Young Patients Treated with Clopidogrel after Myocardial Infarction: A Cohort Study. *The Lancet* **2009**, *373* (9660), 309–317.

(8) Trenk, D.; Hochholzer, W.; Fromm, M. F.; Chialda, L.-E.; Pahl, A.; Valina, C. M.; Stratz, C.; Schmiebusch, P.; Bestehorn, H.-P.; Büttner, H. J.; Neumann, F.-J. Cytochrome P450 2C19 681G>A Polymorphism and High On-Clopidogrel Platelet Reactivity Associated With Adverse 1-Year Clinical Outcome of Elective Percutaneous Coronary Intervention With Drug-Eluting or Bare-Metal Stents. *J. Am. Coll. Cardiol.* **2008**, *51* (20), 1925–1934.

(9) Giusti, B.; Gori, A. M.; Marcucci, R.; Saracini, C.; Sestini, I.; Paniccia, R.; Buonamici, P.; Antoniucci, D.; Abbate, R.; Gensini, G. F. Relation of Cytochrome P450 2C19 Loss-of-Function Polymorphism to Occurrence of Drug-Eluting Coronary Stent Thrombosis. *Am. J. Cardiol.* **2009**, *103* (6), 806–811.

(10) Claassens, D. M. F.; Vos, G. J. A.; Bergmeijer, T. O.; Hermanides, R. S.; van 't Hof, A. W. J.; van der Harst, P.; Barbato, E.; Morisco, C.; Tjon Joe Gin, R. M.; Asselbergs, F. W.; Mosterd, A.; Herrman, J.-P. R.; Dewilde, W. J. M.; Janssen, P. W. A.; Kelder, J. C.; Postma, M. J.; de Boer, A.; Boersma, C.; Deneer, V. H. M.; ten Berg, J. M. A Genotype-Guided Strategy for Oral P2Y 12 Inhibitors in Primary PCI. *N. Engl. J. Med.* **2019**, *381* (17), 1621–1631.

(11) Pereira, N. L.; Farkouh, M. E.; So, D.; Lennon, R.; Geller, N.; Mathew, V.; Bell, M.; Bae, J.-H.; Jeong, M. H.; Chavez, I.; Gordon, P.; Abbott, J. D.; Cagin, C.; Baudhuin, L.; Fu, Y.-P.; Goodman, S. G.; Hasan, A.; Iturriaga, E.; Lerman, A.; Sidhu, M.; Tanguay, J.-F.; Wang, L.; Weinshilboum, R.; Welsh, R.; Rosenberg, Y.; Bailey, K.; Rihal, C. Effect of Genotype-Guided Oral P2Y12 Inhibitor Selection vs Conventional Clopidogrel Therapy on Ischemic Outcomes After Percutaneous Coronary Intervention: The TAILOR-PCI Randomized Clinical Trial. *JAMA* **2020**, *324* (8), 761–771.

(12) European Medicines Agency. Camzyos, INN Mavacamten: Summary of Product Characteristics . In *Summary of Product Characteristics EU/1/23/1716/001-012*; European Medicines Agency: Amsterdam, **2023**. https://www.ema.europa.eu/en/documents/product-information/camzyos-epar-product-information_en.pdf (accessed Dec 05, 2025).

(13) Braunwald, E.; Saberi, S.; Abraham, T. P.; Elliott, P. M.; Olivotto, I. Mavacamten: A First-in-Class Myosin Inhibitor for Obstructive Hypertrophic Cardiomyopathy. *Eur. Heart J.* **2023**, *44* (44), 4622–4633.

(14) Magavern, E. F.; McDermott, J. H.; Caulfield, M. J.; Newman, W. G. CYP2C19 Genetic Testing for Mavacamten and Ischaemic Stroke Treatment: What Does the Result Mean for Cardiovascular Prescribers in the UK and Europe?. *Eur. Heart J.: Cardiovasc. Pharmacother.* **2024**, *10* (6), 481–483.

(15) Lebreton, L.; Boyer, J.; Lafay-Chebassier, C.; Hennart, B.; Baklouti, S.; Cunat, S.; Vilquin, P.; Medard, Y.; Gautier-Veyret, E.; Laffitte-Redondo, C.; Verstuyft, C.; Ait Tayeb, A. E. K.; Haufroid, V.; Wils, J.; Lamoureux, F.; Evrard, A.; Davaze-Schneider, J.; Ben-Sassi, M.; Picard, N.; Quaranta, S.; Ayme-Dietrich, E.; French-Speaking Network of Pharmacogenetics (RNPGx) French-Speaking Network of Pharmacogenetics (RNPGx) Recommendations for Clinical Use of Mavacamten. *Clin. Pharmacol. Ther.* **2025**, *117* (2), 387–397.

(16) Patel, T. J.; Wehbe, E.; Hughes, S.; Patanwala, A. E.; Kritharides, L.; Lal, S.; Patel, S.; Stocker, S. L. Implementing CYP2C19-Guided Clopidogrel Therapy: A Scoping Review of Pharmacogenomic Testing Services. *Pharmacogenomics J.* **2025**, *25* (3), 12.

(17) Kaminski, M. M.; Abudayyeh, O. O.; Gootenberg, J. S.; Zhang, F.; Collins, J. J. CRISPR-Based Diagnostics. *Nat. Biomed. Eng.* **2021**, *5* (7), 643–656.

(18) Liu, G. Advancing CRISPR/Cas Biosensing with Integrated Devices. *ACS Sens.* **2025**, *10* (2), 575–576.

(19) Dai, Y.; Wu, Y.; Liu, G.; Gooding, J. J. CRISPR Mediated Biosensing Toward Understanding Cellular Biology and Point-of-Care Diagnosis. *Angew. Chem., Int. Ed.* **2020**, *59* (47), 20754–20766.

(20) Veer, H. J.Van Der; Aalen, E. A.Van; Michielsen, C. M. S.; Hanckmann, E. T. L.; Deckers, J.; Borren, M. M. G. J.Van; Flipse, J.; Loonen, A. J. M.; Schoeber, J. P. H.; Merkx, M. Glow-in-the-Dark Infectious Disease Diagnostics Using CRISPR-Cas9-Based Split Luciferase Complementation. *ACS Cent. Sci.* **2023**, *9* (4), 657–667.

https://doi.org/10.1021/acssensors.6c00841
ACS Sens. XXXX, XXX, XXX–XXX

(21) Kaminski, M. M.; Alcantar, M. A.; Lape, I. T.; Greensmith, R.; Huske, A. C.; Valeri, J. A.; Marty, F. M.; Klämbt, V.; Azzi, J.; Akalin, E.; Riella, L. V.; Collins, J. J. A CRISPR-Based Assay for the Detection of Opportunistic Infections Post-Transplantation and for the Monitoring of Transplant Rejection. *Nat. Biomed. Eng.* **2020**, *4* (6), 601–609.
(22) Greensmith, R.; Lape, I. T.; Riella, C. V.; Schubert, A. J.; Metzger, J. J.; Dighe, A. S.; Tan, X.; Hemmer, B.; Rau, J.; Wendlinger, S.; Diederich, N.; Schütz, A.; Riella, L. V.; Kaminski, M. M. CRISPR-Enabled Point-of-Care Genotyping for APOL1 Genetic Risk Assessment. *EMBO Mol. Med.* **2024**, *16* (10), 2619–2637.
(23) Ghouneimy, A.; Mahas, A.; Marsic, T.; Aman, R.; Mahfouz, M. CRISPR-Based Diagnostics: Challenges and Potential Solutions toward Point-of-Care Applications. *ACS Synth. Biol.* **2023**, *12* (1), 1–16.
(24) Kumar, M.; Maiti, S.; Chakraborty, D. Capturing Nucleic Acid Variants with Precision Using CRISPR Diagnostics. *Biosens. Bioelectron.* **2022**, *217*, No. 114712.
(25) Chen, Y.; Mei, Y.; Jiang, X. Universal and High-Fidelity DNA Single Nucleotide Polymorphism Detection Based on a CRISPR/Cas12a Biochip. *Chem. Sci.* **2021**, *12* (12), 4455–4462.
(26) Wu, Y.; Liu, Y.; Chang, Y.; Liu, M. Integration of CRISPR/Cas13a and V-Shape PCR for Rapid, Sensitive, and Specific Genotyping of CYP2C19 Gene Polymorphisms. *Anal. Chem.* **2023**, *95* (26), 10127–10135.
(27) Wu, Y.; Jin, R.; Chang, Y.; Liu, M. A High-Fidelity DNAzyme-Assisted CRISPR/Cas13a System with Single-Nucleotide Resolved Specificity. *Chem. Sci.* **2024**, *15* (18), 6934–6942.
(28) Mai, Z.; Zhou, T.; Lin, Z. Detecting CYP2C19 Genes through an Integrated CRISPR/Cas13a-Assisted System. *Anal. Methods* **2025**, *17* (6), 1382–1388.
(29) Wu, X.; Luo, S.; Guo, C.; Zhao, Y.; Zhong, J.; Hu, R.; Yang, X.; Liu, C.; Zhang, Q.; Zhuang, S.; Chen, Y.; Liu, Y.; Zhang, X. LbuCas13a Directly Targets DNA and Elicits Strong Trans-Cleavage Activity. *Nat. Biomed. Eng.* **2025**, *9* (12), 2141–2154.
(30) Luo, S.; Chen, Y.; Li, Z.; Zhang, X.; Liu, Y. Single-Tube Lambda Exonuclease-Mediated LbuCas13a Detect of ssDNA for Single-Nucleotide Polymorphisms Genotyping. *Biosens. Bioelectron.* **2025**, *288*, No. 117760.
(31) Gootenberg, J. S.; Abudayyeh, O. O.; Lee, J. W.; Essletzbichler, P.; Dy, A. J.; Joung, J.; Verdine, V.; Donghia, N.; Daringer, N. M.; Freije, C. A.; Myhrvold, C.; Bhattacharyya, R. P.; Livny, J.; Regev, A.; Koonin, E. V.; Hung, D. T.; Sabeti, P. C.; Collins, J. J.; Zhang, F. Nucleic Acid Detection with CRISPR-Cas13a/C2c2. *Science* **2017**, *356* (6336), 438–442.
(32) Gootenberg, J. S.; Abudayyeh, O. O.; Kellner, M. J.; Joung, J.; Collins, J. J.; Zhang, F. Multiplexed and Portable Nucleic Acid Detection Platform with Cas13, Cas12a, and Csm6. *Science* **2018**, *360* (6387), 439–444.
(33) Kellner, M. J.; Koob, J. G.; Gootenberg, J. S.; Abudayyeh, O. O.; Zhang, F. SHERLOCK: Nucleic Acid Detection with CRISPR Nucleases. *Nat. Protoc.* **2019**, *14* (10), 2986–3012.
(34) Arizti-Sanz, J.; Freije, C. A.; Stanton, A. C.; Petros, B. A.; Boehm, C. K.; Siddiqui, S.; Shaw, B. M.; Adams, G.; Kosoko-Thoroddsen, T.-S. F.; Kemball, M. E.; Uwanibe, J. N.; Ajogbasile, F. V.; Eromon, P. E.; Gross, R.; Wronka, L.; Caviness, K.; Hensley, L. E.; Bergman, N. H.; MacInnis, B. L.; Happi, C. T.; Lemieux, J. E.; Sabeti, P. C.; Myhrvold, C. Streamlined Inactivation, Amplification, and Cas13-Based Detection of SARS-CoV-2. *Nat. Commun.* **2020**, *11* (1), No. 5921.
(35) Meng, X.; Wang, A.; Zhang, G.; Niu, S.; Li, W.; Han, S.; Fang, F.; Zhao, X.; Dong, K.; Jin, Z.; Zheng, H.; Chen, K.; Li, H.; Yang, C.; Wang, Y. Analytical Validation of GMEX Rapid Point-of-Care CYP2C19 Genotyping System for the CHANCE-2 Trial. *Stroke Vasc. Neurol.* **2021**, *6* (2), 274–279.
(36) Rohland, N.; Reich, D. Cost-Effective, High-Throughput DNA Sequencing Libraries for Multiplexed Target Capture. *Genome Res.* **2012**, *22* (5), 939–946.
(37) Chen, P.; Zhou, J.; Wan, Y.; Liu, H.; Li, Y.; Liu, Z.; Wang, H.; Lei, J.; Zhao, K.; Zhang, Y.; Wang, Y.; Zhang, X.; Yin, L. A Cas12a Ortholog with Stringent PAM Recognition Followed by Low Off-Target Editing Rates for Genome Editing. *Genome Biol.* **2020**, *21* (1), No. 78.
(38) Zhou, J.; Chen, P.; Wang, H.; Liu, H.; Li, Y.; Zhang, Y.; Wu, Y.; Paek, C.; Sun, Z.; Lei, J.; Yin, L. Cas12a Variants Designed for Lower Genome-Wide off-Target Effect through Stringent PAM Recognition. *Mol. Ther.* **2022**, *30* (1), 244–255.
(39) Lewis, J. P.; Backman, J. D.; Reny, J.-L.; Bergmeijer, T. O.; Mitchell, B. D.; Ritchie, M. D.; Déry, J.-P.; Pakyz, R. E.; Gong, L.; Ryan, K.; Kim, E.-Y.; Aradi, D.; Fernandez-Cadenas, I.; Lee, M. T. M.; Whaley, R. M.; Montaner, J.; Gensini, G. F.; Cleator, J. H.; Chang, K.; Holmvang, L.; Hochholzer, W.; Roden, D. M.; Winter, S.; Altman, R. B.; Alexopoulos, D.; Kim, H.-S.; Gawaz, M.; Bliden, K. P.; Valgimigli, M.; Marcucci, R.; Campo, G.; Schaeffeler, E.; Dridi, N. P.; Wen, M.-S.; Shin, J. G.; Fontana, P.; Giusti, B.; Geisler, T.; Kubo, M.; Trenk, D.; Siller-Matula, J. M.; Ten Berg, J. M.; Gurbel, P. A.; Schwab, M.; Klein, T. E.; Shuldiner, A. R.; et al. Pharmacogenomic Polygenic Response Score Predicts Ischaemic Events and Cardiovascular Mortality in Clopidogrel-Treated Patients. *Eur. Heart J.: Cardiovasc. Pharmacother.* **2020**, *6* (4), 203–210.
(40) Lee, C. R.; Thomas, C. D.; Beitelshees, A. L.; Tuteja, S.; Empey, P. E.; Lee, J. C.; Limdi, N. A.; Duarte, J. D.; Skaar, T. C.; Chen, Y.; Cook, K. J.; Coons, J. C.; Dillon, C.; Franchi, F.; Giri, J.; Gong, Y.; Kreutz, R. P.; McDonough, C. W.; Stevenson, J. M.; Weck, K. E.; Angiolillo, D. J.; Johnson, J. A.; Stouffer, G. A.; Cavallari, L. H.; IGNITE Network Pharmacogenetics Working Group. Impact of the CYP2C19*17 Allele on Outcomes in Patients Receiving Genotype-Guided Antiplatelet Therapy After Percutaneous Coronary Intervention. *Clin. Pharmacol. Ther.* **2021**, *109* (3), 705–715.

https://doi.org/10.1021/acssensors.6c00841
ACS Sens. XXXX, XXX, XXX–XXX